

Statistical variations of the elementary flux-pinning force and their effect on the shape of the bulk-pinning-force curve of high-field superconductors

L. D. Cooley, G. Stejic,* and D. C. Larbalestier*,†

Applied Superconductivity Center, University of Wisconsin, 1500 Johnson Drive, Madison, Wisconsin 53706

(Received 18 February 1992)

It is a common procedure to infer the flux-pinning mechanism from the shape of the bulk-pinning-force curve $[F_p(b)]$. In this paper, we investigate the effects of having a distribution of elementary pinning forces (f_p) on $F_p(b)$ within the framework of fluxon core pinning and full summation. It is seen that the shape of $F_p(b)$ can be significantly changed when the pins are strong and their f_p distribution broad, whereas traditional ideas accept that its shape remains constant. A shift of the peak of $F_p(b)$ to lower field and an increase in the curvature of the high-field portion of $F_p(b)$ is seen. We find confirmation of the model in optimized high- J_c Nb-Ti composites, which have a broad distribution of α -Ti precipitate thicknesses.

I. INTRODUCTION

The bulk pinning force F_p (N/m³) is a very important characteristic of a type-II superconductor. The higher F_p is, the larger the current-carrying capacity of a superconductor is, and the more useful it is technologically. In theory, F_p is separable into three terms that are functions only of the microstructure, temperature, and reduced field $b \equiv B/B_{c2}$, respectively,¹

$$F_p(M, T, b) = g(M) B_{c2}^m(T) b^p (1-b)^q. \quad (1)$$

In principle one can obtain an expression for each term based on knowledge of the microstructure, hypotheses concerning the pinning mechanism(s) operating for that microstructure,²⁻⁹ and the way in which the elementary pinning forces $f_p(M, T, b)$ are summed to create the bulk pinning force.¹⁰⁻¹³ It is also common to undertake the inverse procedure, namely to measure the field and/or temperature dependence of F_p and then to deduce the pinning mechanism(s) that might be in operation.¹⁴⁻¹⁷ A consistent picture sometimes emerges when the microstructure contains a dominant pinning defect, for example grain boundaries in Nb₃Sn (Ref. 9) or core pinning by titanium precipitates in Nb-Ti composites,^{17,18} although deviations from the predicted scaling function may also be observed.^{17,19} However, several species of defects can frequently be identified in the microstructure, and the development of a consistent picture of the flux-pinning mechanisms is in general quite complicated. This is particularly the case for single crystal YBa₂Cu₃O_{7- δ} , where the dominant flux-pinning mechanisms have variously been proposed as oxygen vacancies in the CuO₂ planes,²⁰ ordered oxygen vacancies in the CuO chains,²¹ modulations of the shear modulus of the flux lattice,²² twin planes and stacking faults,²³ and "intrinsic" pinning by weakly superconducting non-CuO₂ layers.²⁴

A deviation in the field dependence of F_p from its predicted functional form is, therefore, often interpreted as an indication of a change in the elementary pinning

mechanism (see, for example, Refs. 17 and 25). However, sometimes such a conclusion is not reconcilable with the microstructural data and our understanding of the types of pinning mechanisms that are associated with various defects. A good example is found in optimized Nb 44–62 wt. % Ti alloys^{17,18,26} where, despite the clear domination of a single microstructural defect (Ti precipitates), as well as convincing evidence for both the operation of a strong, core-pinning interaction and for direct summation, the expected $b(1-b)$ scaling function is not observed at all temperatures. The shape of the $F_p(b)$ curve is consistent with the prediction at low temperatures, but changes at $T/T_c \gtrsim 0.6$ produce a pinning function having its peak at a progressively lower field and developing more curvature in the high-field region. We have paid particular attention to the details of flux pinning in the Nb-Ti system because it is, in principle, possible to make both a detailed microstructural analysis and a complete electromagnetic analysis.^{17,18} The apparent failure of temperature scaling in this system is thus valuable to the discussion of the validity of flux-pinning models.

In this paper, we address this potential problem by proposing that changes in the field dependence of F_p can occur, even though a single pinning mechanism remains operative. Our model proposes that the filling of a distribution of pinning forces occurs preferentially. This occurs because a given fluxon samples a larger effective volume when the field is low, than when the field is high. The fluxon may then be able to occupy an especially strong subset of pins at low field, whereas it is forced to settle for a more random sampling of pins at high field. We consider here only a pin density that is high enough so that direct (full) summation holds, allowing us to apply this single-fluxon model for f_p to the bulk pinning force. This results in an extra field dependence of $F_p(b)$ that is connected to this filling of the pin distribution, in addition to the particular field dependences of the pinning mechanism and of the summation scheme. We develop our description first in a general fashion, later connecting it directly to the specifics of pinning in the Nb-Ti system,

where we have developed an extensive knowledge base over a wide range of compositions and pin densities.^{17,18,26-29} We note that the concept of a pin distribution with a preferential hierarchy has been considered by several authors,³⁰⁻³⁴ although none has been applied to the bulk pinning force. This paper extends our earlier work³⁵ on its application to the field dependence of F_p .

II. DESCRIPTION OF THE MODEL

In order to achieve a high current density or bulk pinning force, one attempts to create a microstructure that can pin every fluxon effectively. The strongest elementary pinning force arises from core pinning,^{2,3,36} where $f_p \propto 1-b$. This means that the wavelength of microstructural variations must be comparable to the coherence length ξ and the mean separation between fluxons

$$a_0 \approx 1.07(\phi_0/B)^{1/2} \approx 2.69\xi/\sqrt{b}.$$

This implies that long-range variations in the microstructure (on the order of the magnetic penetration depth, λ) are of lesser importance. In the optimum case, the pins are so densely arranged that the response of the fluxon lattice to the pinning distortions is highly nonlocal.³⁷⁻³⁹ As pointed out by Brandt,³⁸ the magnetic-field lines cannot then follow the trajectory of the vortex cores. Several consequences ensue.

(1) The elastic energy increase accompanying an *abrupt* deviation (a few ξ in length) of a fluxon core onto a pin is smaller than that of a *gradual* deviation (nearly λ in length) by a factor of order $1/\kappa^2$. Given that high-field superconductors have κ values of order 20 (Al₅ compounds), 45 (Nb 47 wt. % Ti), or even higher for high-temperature superconductors, this reduction factor can be very large. Thus, in a high- κ superconductor with a high density of strong pins, abrupt deviations will occur often. A high- κ superconductor with weaker or more widely spaced pins (but such that direct summation still holds) will be accompanied by more gradual deviations.

(2) Abrupt distortions of the core contribute energy only by lengthening the fluxon core; the magnetic energy does not change, because the field lines are not influenced by the distortions. This energy is $\epsilon_1 = 4 \ln(\kappa)\epsilon_0$ per unit of length increase caused by the distortion, where $\epsilon_0 = \mu_0 H_c^2 \pi \xi^2$. This energy change is independent of field.

(3) The energy of a gradual distortion is dominated by the magnetic interaction with other fluxons, contributing an energy $\sim (1 + \kappa^2 b)\epsilon_0$ per unit length of the distortion.

(4) The field at which a crossover from the nonlocal regime in (2) to the more local regime in (3) occurs is difficult to determine. However, it will in general be higher as the pins are made stronger.

Based on these ideas, we can make several generalizations about the fluxon-pin interactions in strongly pinning superconductors at low field.

(1) Substantial lateral deviations of fluxon cores perpendicular to the field vector will occur in order to occupy a pin.

(2) Pinning interactions are not correlated with each other along the length of the fluxon.

(3) The pinning interactions of a given fluxon are in-

dependent of those of its neighbors.

(4) The wavelength of pinning interactions along the length of a fluxon may approach the average spacing of pins in the microstructure.

(5) As the field increases, the wavelength of a given deviation increases in order to offset the decreasing pin strength.

Since the real microstructure of a superconductor is not perfectly uniform, variations in pin size, spacing, composition, and concentration are expected, and should be described in terms of distribution functions. The elementary pinning force can also then be described by a distribution function, $N[f_p(b)]$, for given b . In a superconductor with a high density of pins, a fluxon will be able to choose which of several pins to occupy at low field, because the pin spacing is much smaller than the mean fluxon spacing. For example, in Nb 48 wt. % Ti the pin spacing is $\sim 2.2\xi$, ≈ 11 nm at 4.2 K for 20 vol % of pins, a level that is readily attainable,^{28,29} while $a_0 \approx 49$ nm at 1 T, $\approx 0.1B_{c2}$. It follows that the strongest pins are occupied with highest probability. Several schemes for the filling of the pin distribution as the number of fluxons increases can thus be envisioned, as sketched in Fig. 1. In general, the stronger the pins are, the more the distribution of occupied pins (the shaded regions in Fig. 1) changes from a random distribution to one with a preferential hierarchy. An alternate way to think of this is to imagine the occupied pins as fermions, since there is an effective exclusion principle governing the occupation of pins,³² so that the distribution of $f_p(b)$ for the occupied pins is approximately the product of $N[f_p(b)]$ and a Fermi-like probability function,

$$N[f_p(b)]_{\text{occ}} \approx N[f_p(b)] \left[1 - \frac{1}{1 + \exp\{[f_p(b) - f_{pm}(b)]/\tilde{T}\}} \right], \quad (2)$$

where $f_{pm}(b)$ is analogous to the chemical potential of the fluxons. The parameter \tilde{T} is the "temperature" of the pins: since strong pins are not expected to have an appreciable "excitation spectrum," they have a lower "temperature" than weak pins.

At a given field, the pinning force per fluxon, $\approx (\phi_0/B)F_p$, is the sum of the elementary pinning forces along the length of the fluxon. In the dense-pinning limit, it is proportional to the mean value of f_p for the occupied pins $\langle f_p(b) \rangle_{\text{occ}}$. However, because of preferential filling of the pin distribution, $\langle f_p \rangle_{\text{occ}}$ may be significantly larger than the mean value of the entire distribution $\langle f_p(b) \rangle = f_{p0}(1-b)$, where f_{p0} is the average elementary pinning force at zero field. This is indicated in Fig. 1. When the filling is optimum, that is, when the strongest available pins are always occupied first, the highest value of $\langle f_p \rangle_{\text{occ}}$ is obtained, $\langle f_p(b) \rangle_{\text{opt}}$. We can predict two trends. First, as f_{p0} is increased, the difference between $\langle f_p \rangle_{\text{occ}}$ and $\langle f_p \rangle$ increases because the filling of the f_p distribution is more preferential. This is depicted in plots (a), (b), and (c) of Fig. 1. Second, as the f_p distribution

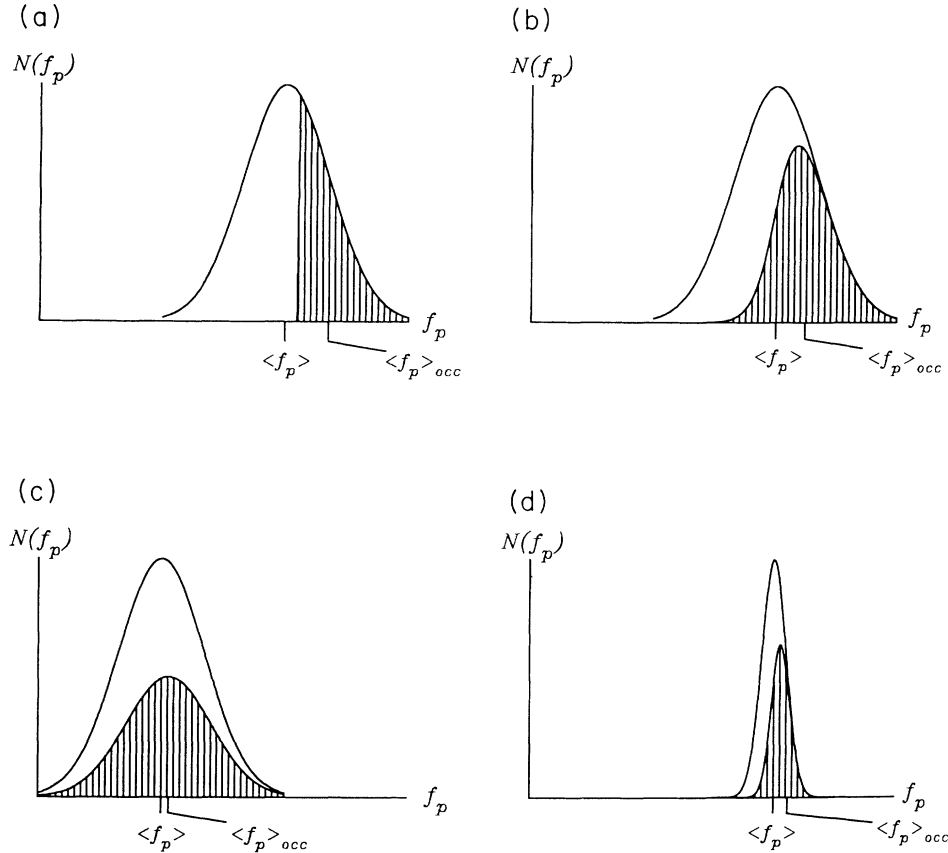


FIG. 1. Schematic representation of various ways in which a distribution of pin strengths can be filled. $N(f_p)$ is the distribution of the elementary pinning force f_p . Representative values of $\langle f_p \rangle$ and $\langle f_p \rangle_{occ}$ are indicated. (a) Optimum filling (hatched region) of a broad distribution, in which the strongest remaining unoccupied pins are always occupied first. (b) A possible filling scheme of a broad distribution of strong pins. (c) Possible filling scheme of a broad distribution of weak pins. (d) Filling of a narrow distribution of strong pins.

gets broader, the differences between $\langle f_p \rangle_{opt}$ and $\langle f_p \rangle_{occ}$ and between $\langle f_p \rangle_{opt}$ and $\langle f_p \rangle$ increase. Further, for any distribution and any filling scheme, $\langle f_p \rangle_{opt}$, $\langle f_p \rangle_{occ}$, and $\langle f_p \rangle$ must all be equal as $b \rightarrow 1$. Therefore, the field dependence of the *real* pinning force on a fluxon, being proportional to $\langle f_p \rangle_{occ}$, must be *more strongly decreasing* than that of the pinning mechanism, being proportional to $\langle f_p \rangle$.

When a link between F_p and a pinning mechanism is sought, generally the field and temperature dependences of f_p that are obtained from various flux-pinning theories are assembled and compared to the observed properties, using Eq. (1). However, unless a great effort is taken to account for variations in the microstructure, these calculations use average values for the microstructural parameters, i.e., the calculated $f_p = \langle f_p \rangle$. Since the observed properties of F_p are in reality dependent on $\langle f_p \rangle_{occ}$ and not $\langle f_p \rangle$, it follows that the field dependences of F_p and $\langle f_p \rangle$ are *not* alike. This leaves open the possibility that an observable variation in the shape of the $F_p(b)$ curve may occur *even though a single pinning mechanism is operative*, as well as the possibility that the pinning mechanism may be misidentified.

The purpose of this paper is to estimate the low-field

difference between $\langle f_p \rangle_{occ}$ and $\langle f_p \rangle$ and the extra field dependence of F_p , which subsequently results. We calculate $\langle f_p \rangle_{occ}$ using a numerical simulation. The extra field dependence is expressed in the function $P(b)$ by subtracting the values of $\langle f_p \rangle$, which are based on a core-pinning model [recall that $\langle f_p \rangle = f_{p0}(1-b)$], from the calculated values of $\langle f_p \rangle_{occ}$ for a range of fields $b = 0.1-0.9$. This gives

$$\langle f_p(b) \rangle_{occ} = \frac{\langle f_p(0) \rangle_{occ}}{f_{p0}} (1-b) P(b). \quad (3)$$

As the results will show, $P(b) \approx 1$ for all b when the microstructure is very uniform and the pins are weak, but $P(b)$ becomes a stronger function, $\sim (1-b)$, when the microstructure has large variations and the pins are strong. When $P(b) \approx 1$ for a large range of b , the field dependence of $\langle f_p \rangle_{occ}$ is very close to the calculated field dependence, as would be expected. On the other hand, when $P(b)$ is strongly field dependent, $\langle f_p \rangle_{occ}$ becomes more strongly field dependent than $\langle f_p \rangle$. Using our core-pinning example, we have $\langle f_p(b) \rangle \propto (1-b)$ and if $P(b) = 1-b$, then $\langle f_p \rangle_{occ} \propto (1-b)^2$. The field dependence of F_p is then given by

$$F_p(b) \approx \frac{B_{c2}}{\phi_0} b \langle f_p(b) \rangle_{\text{occ}} \propto b(1-b)P(b). \quad (4)$$

This gives $F_p \propto b(1-b)^2$ for the above example, in comparison to the expected $b(1-b)$ function. This distinction is not at all trivial, since $F_p \propto (1-b)^2$ represents the general behavior expected from fluxon lattice shear, as in the A15 compounds,⁴ while $F_p \propto (1-b)$ represents the conceptually quite different *individual* fluxon depinning normally observed in optimized Nb-Ti alloys. The finding that *both* functions could operate in optimized Nb-Ti alloys in different temperature ranges^{17,27} was a major surprise.

III. DESCRIPTION OF THE CALCULATIONS

$P(b)$ is simulated numerically by placing a model fluxon parallel to a two-dimensional array of pins and iteratively displacing a portion of its length perpendicular to its path. Only the two-dimensional array has been tested; the three-dimensional case is currently under investigation. The perturbations were applied at a random location along the fluxon's length and occurred randomly in one direction or the other. The progression of fluxon configurations was determined by accepting perturbations that minimized the effective energy of the fluxon,

$$E = L - U, \quad (5)$$

where L is the line energy added by the perturbation and U is the pinning energy if a local pinning interaction occurs, until a configuration of lowest energy was obtained. This configuration was then used to calculate the quantities of interest in the experiment, as will be described shortly.

The simulated pins were square, being one coherence length on a side. The average separation s of the pins was determined by the volume fraction of pins used; we report here the results for 20% of pins. The positions of the pins were then slightly adjusted at random in order to model the variability that exists in a real microstructure. A pinning energy was assigned to each pin using a Gaussian distribution with specified values of the mean and the coefficient of variation (COV). Values of the mean were chosen to be in the range 0.1–1.0, in units of ϵ_0 (J/m). The value of f_{p0} was then determined by dividing the mean pinning energy by ξ ; the values of f_{p0} were thus 0.1–1.0, in units of ϵ_0/ξ (N/m). The range of COV values was 0.1–0.50. The field-dependent strength of each pin was chosen to be $\propto (1-b)$, in accordance with a core-pinning model, for the range $b = 0.1$ –0.9.

A straight, 10λ -long model fluxon was placed in the center of the array at the start of each run. The fluxon cross section was modeled as a vee, the strength of a pinning intersection being maximum for the center coordinate and falling off linearly to zero over a distance ξ from the center. The free energy was calculated by applying Eq. (5) for each fluxon-pin intersection along the length of the fluxon, where the interactions were considered individually. The line energy was calculated by multiplying the change in the length of the fluxon by ϵ_1 , using $\kappa = 40$.

The perturbations were generated iteratively in two

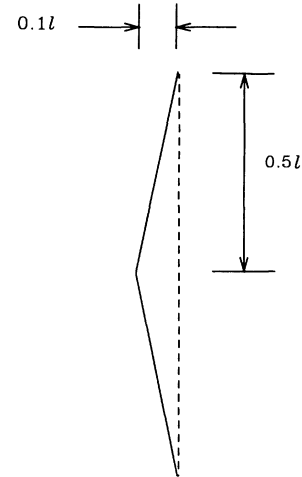


FIG. 2. Schematic of the triangular perturbations applied to the model fluxon.

passes, each using a triangular displacement of the fluxon applied at a random location along its length. For the first pass, the perturbation extended for a distance $0.5l$ (the wave number $k = \pi/l$) in either direction along the

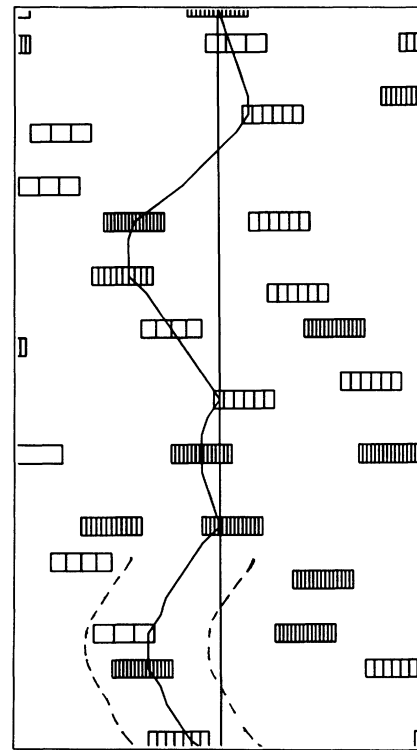


FIG. 3. The initial and final position of the center of the model fluxon illustrated by the straight and crooked lines, respectively. The shaded rectangles represent the pins, where the stronger pins have a darker shading. The dashed lines at the bottom of the figure indicate the diameter of the fluxon core. The vertical axis has been compressed by a factor of 3.3 (the pins are actually square), so that a region of approximately a_0 by λ (6.5 by 40ξ) is shown. The simulation shown here is for $f_{p0} = 1.0$, $b = 0.2$, and a coefficient of variation of 0.5.

fluxon and had an amplitude at the center of the perturbation of $0.1l$ as Fig. 2 shows. The value of l was determined either by setting the dispersive factor in the tilt modulus of the flux lattice,³⁷⁻³⁹ $k\lambda/(1-b)^{1/2}$ equal to 10, giving a field-dependent value of $l \approx 4.5-9\xi$ for the fields tested, or by setting $l = 2s \approx 6\xi$. The results did not appear to depend on the choice of perturbation wavelength. If the free energy of the perturbed fluxon was lower than that of the unperturbed fluxon, the perturbation was made permanent for subsequent iterations. Convergence to a stable configuration occurred when none of the grid positions assigned to the fluxon could be further displaced and still reduce the free energy. No restriction was placed on the ultimate local displacements which the fluxon core could make from its starting position, however the maximum deviation that was observed was $0.32a_0$.

In the second pass, l was reduced to one coherence length, starting from the stable configuration obtained upon the completion of the first pass. The displacement amplitude was reduced to 0.1ξ . Finally, $\langle f_p \rangle_{\text{occ}}$ was calculated by dividing the free energy of the final configuration by ξ . Then, $P(b)$ was obtained by analyzing the initial and final configurations and comparing the corresponding values of $\langle f_p \rangle_{\text{occ}}$. We observed that the initial value of $\langle f_p \rangle_{\text{occ}}$ (i.e., a random sampling of the pins) was always within 1% of the theoretical starting value f_{p0} . Figure 3 shows the starting and final configurations for the center coordinate of the model fluxon for $b = 0.2$, $f_{p0} = 1.0$, and a COV of 0.5.

IV. RESULTS

The results of the calculations of $\langle f_p \rangle_{\text{occ}}$ for weak pins, $f_{p0} = 0.1$, are shown in Fig. 4 as a function of b with

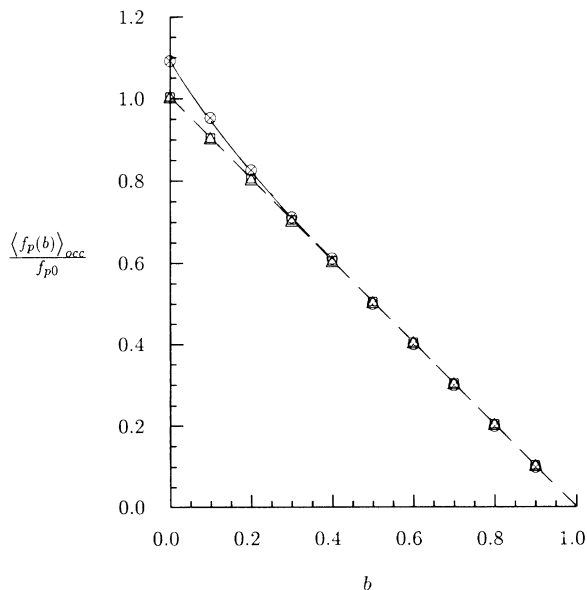


FIG. 4. Calculated values of $\langle f_p(b) \rangle_{\text{occ}}$ using weak pins ($f_{p0} = 0.1$), for increasing coefficients of variation. The data has been normalized to the value of f_{p0} . The coefficients of variation are 0.01 (\square), 0.1 (\triangle), and 0.5 (\otimes). The value of $\langle f_p \rangle_{\text{occ}}$ at $b = 0$ is extrapolated from the higher-field points. The dashed line indicates the field dependence of $\langle f_p(b) \rangle$ that would be expected from core pinning alone ($\propto 1-b$).

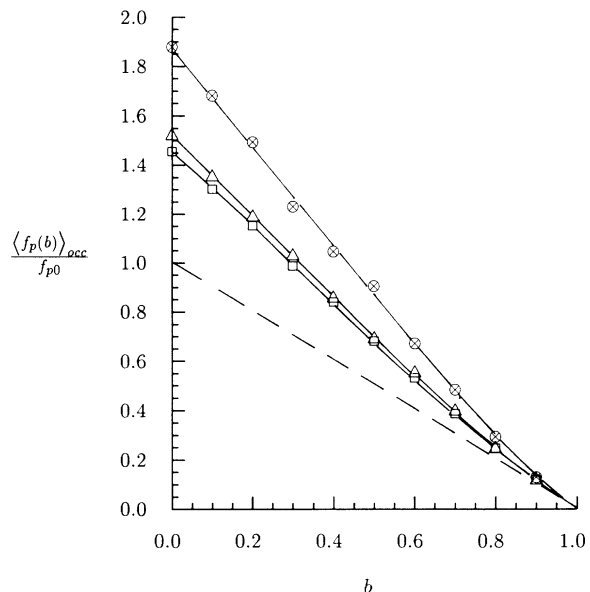


FIG. 5. Calculated values of $\langle f_p(b) \rangle_{\text{occ}}$ using strong pins ($f_{p0} = 2.0$), for increasing coefficients of variation. The data has been normalized to the value of f_{p0} . The coefficients of variation are 0.01 (\square), 0.1 (\triangle), and 0.5 (\otimes). The value of $\langle f_p \rangle_{\text{occ}}$ at $b = 0$ is extrapolated from the higher-field points. The dashed line indicates the field dependence of $\langle f_p(b) \rangle$ that would be expected from core pinning alone ($\propto 1-b$).

the coefficients of variation being 0.01, 0.1, and 0.5. The corresponding plot for strong pins, $f_{p0} = 2.0$, is shown in Fig. 5. The values of $\langle f_p \rangle_{\text{occ}}$ at $b = 0$ are extrapolated from the higher-field points in order to provide a comparison with the input values of f_{p0} . The runs for a COV of 0.01 were undertaken in order to estimate the increased

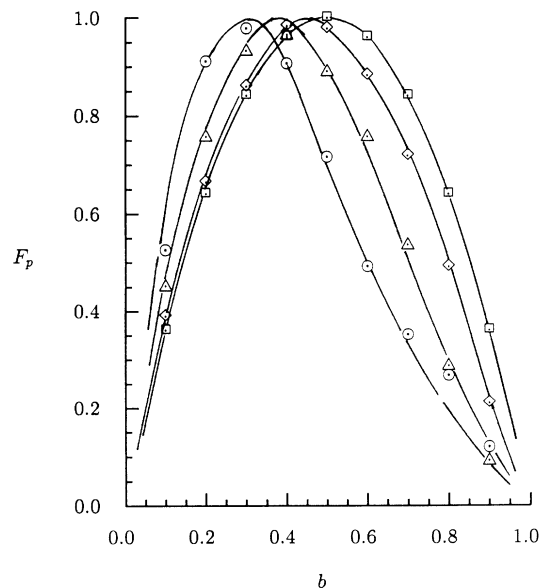


FIG. 6. Normalized $F_p(b)$ curves generated from the $\langle f_p(b) \rangle_{\text{occ}}$ data for f_{p0} and the coefficient of variation values of 0.1, 0.1 (\square); 0.1, 0.5 (\diamond); 2.0, 0.1 (\triangle); and 2.0, 0.5 (\odot), respectively.

TABLE I. Summary of the extrapolated values of $\langle f_p(0) \rangle_{\text{occ}}$.

COV	0.1	0.2	f_{p0} 0.5	1.0	2.0
0.1	1.00	1.06	1.26	1.42	1.52
0.2	1.00	1.12	1.31	1.47	1.45
0.5	1.09	1.35	1.72	1.76	1.88

pinning that occurs when the center of the fluxon core occupies the pin instead of the core's edge, while the higher coefficients were thought to be reasonable values for the types of distributions that might actually be encountered. The enhancement of $\langle f_p \rangle_{\text{occ}}$ at low fields is clearly seen both for weak and strong pins when the COV is large. For strong pins (Fig. 5), the enhancement is seen even for a COV of 0.01, and it becomes more pronounced as the COV increases. Comparing the figures, it is also clear that the enhancement of $\langle f_p \rangle_{\text{occ}}$ occurs as the value of f_{p0} gets larger.

F_p curves were generated from the $\langle f_p \rangle_{\text{occ}}$ data by using the relation in Eq. (4). The four curves corresponding to the combinations of $f_{p0}=0.1$ and 2.0, and the coefficients of variation of 0.1 and 0.5, are summarized in Fig. 6. It is clear that the peak of the $F_p(b)$ curves shifts to lower fields, and that more curvature develops in the high-field regions, as f_{p0} and the COV are increased. A summary of the extrapolated values of $\langle f_p \rangle_{\text{occ}}$ is shown in Table I, and a summary of the field corresponding to the peak in the calculated $F_p(b)$ curves is shown in Table II, for the range of values of f_{p0} and the COV that were used. Again, the data in these tables show the noted trends.

The pinning enhancement function $P(b)$ is plotted in Fig. 7. The data are derived from the data in Figs. 4 and 5, excluding the data for a COV of 0.01. It is clear that the field dependence of the enhancement becomes much stronger as either f_{p0} or the COV increase; the most strongly field-dependent curve occurs when both parameters have a high value.

In Fig. 8, the results for the coefficients of variation 0.01 and 0.50 are compared as a function of f_{p0} . Since there can hardly be any preference toward the occupation of one pin over another when the COV is 0.01, the enhancement of the pinning force must be due to the model fluxon being pulled into the center of the pin, where the deepest part of the vee is figured into the pinning energy. This centering effect appears to increase rapidly at low pinning strengths, and then saturates when

TABLE II. Summary of the fields corresponding to the peak in the calculated $F_p(b)$ curves, b_{max} . The value of b_{max} for $F_p(b) \propto b(1-b)$ is 0.5.

COV	0.1	0.2	f_{p0} 0.5	1.0	2.0
0.1	0.50	0.46	0.39	0.36	0.36
0.2	0.50	0.44	0.40	0.39	0.37
0.5	0.45	0.40	0.35	0.35	0.31

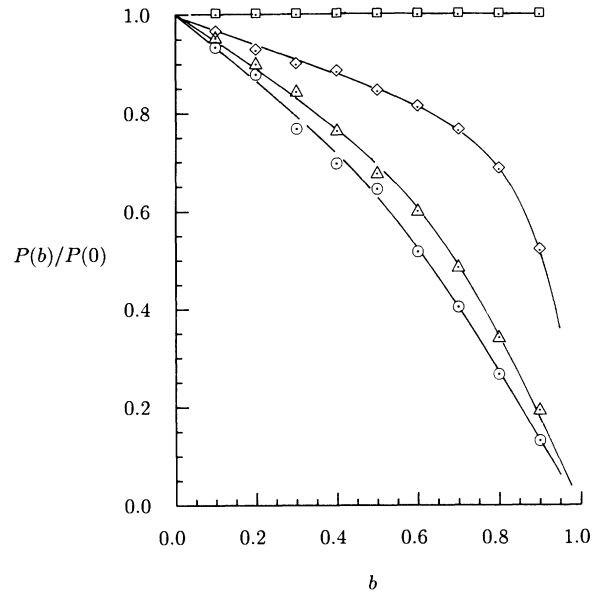


FIG. 7. The pinning enhancement function $P(b)$ plotted for different values of f_{p0} and the coefficient of variation, normalized to the respective values of $P(0)$. The values of $P(0)$ were determined by the ratio $\langle f_p(0) \rangle_{\text{occ}}/f_{p0}$. Here, f_{p0} and the coefficient of variation are 0.1, 0.1 (\square); 0.1, 0.5 (\diamond); 2.0, 0.1 (\triangle); and 2.0, 0.5 (\circ), respectively.

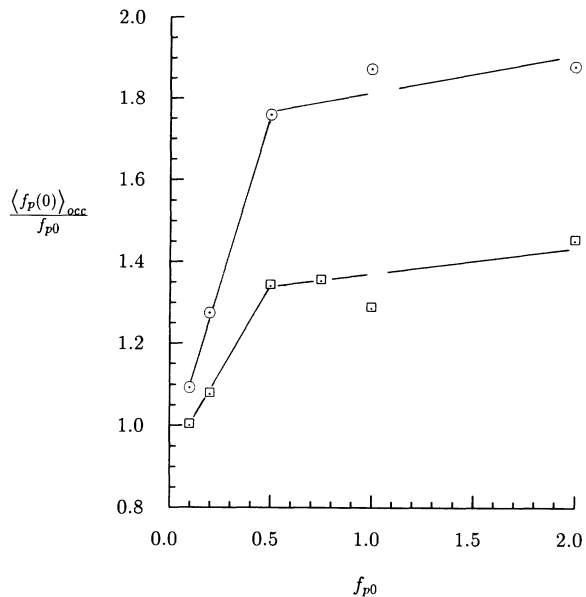


FIG. 8. Variation in the ratio $\langle f_p(0) \rangle_{\text{occ}}/f_{p0}$ as a function of pin strength for a narrow pin strength distribution (the coefficient of variation is 0.01, \square) and a broad pin distribution (the coefficient of variation is 0.5, \circ). The curve for the narrow distribution data indicates the magnitude of the enhancement of $\langle f_p \rangle_{\text{occ}}$ caused by the centering effect, while the difference between the upper and lower curve is the enhancement caused by preferential occupation of the strong pins for the broad distribution.

$f_{p0} \approx 0.5$. This will be discussed in the next section. The additional enhancement that occurs when the COV is 0.5 can be estimated from the difference between the two curves. This rises from about 10% at $f_{p0} = 0.1$ to 35% at $f_{p0} = 1.0$.

V. DISCUSSION

A. The centering effect

The calculated data for the extremely narrow pin distributions (a COV of 0.01) indicate that a substantial enhancement, up to $\sim 35\%$, can be attributed to the tendency of the model fluxon to move toward the center of a strong pin. Since our model pins were one-coherence-length thick, only half of the model fluxon can occupy the pin for any given position, and there will be a 25% increase in the pinning energy when the coordinate of the model fluxon core changes from the edge of the pin to its center. The optimum pinning will occur in this case when the fluxon core sits exactly in the center of every pin that it occupies. This requires a lateral displacement of about 0.5ξ to occur over approximately two pin spacings ($\approx 6\xi$). The corresponding line tension is overcome when $\langle f_p(b) \rangle$ exceeds 0.6, however lower values of $\langle f_p \rangle$ may suffice because of geometric variations in the relative positions of the fluxon core, the pin, and the adjacent segments of the fluxons. This may explain the plateau seen for $f_{p0} \gtrsim 0.5$ in Fig. 8.

A perfect alignment of the fluxons with the pins cannot always occur, because a_0 changes with field. Thus, there is an inherent breadth to the distribution of pinning forces, even if the COV is low. For weak pins, which cannot overcome the line tension, f_p is greater for the pins in which the fluxon is centered. For strong pins, the pins that are not in alignment stretch the fluxon, and their f_p is reduced by the line tension. This means that the actual f_p distribution *always* has a finite width, depending on field and microstructural geometry, even if the pins are themselves all alike (e.g., atomic vacancies or idealized pinning structures). It is not clear what the shape of the f_p distribution would be in the low-COV limit. However, our results indicate that the centering effect can shift the maximum of the core-pinning $F_p(b)$ curve to less than $b = 0.4$.

B. The effect of $P(b)$ on the field dependence of F_p

The results indicate that the enhancement of $\langle f_p \rangle_{\text{occ}}$ at low fields becomes more prevalent as either the COV or f_{p0} is increased. The effect of either parameter on $F_p(b)$ appears to be independent of that of the other, which is supported by the additive nature of the data in Tables I and II. This is in agreement with the model: the COV only affects the shape of the f_p distribution, whereas the value of f_{p0} determines the actual way in which the f_p distribution is filled. If we again consider Eq. (2), then the COV determines the value of $f_{pm}(b)$, whereas the value of f_{p0} affects \tilde{T} . These results suggest that the largest change in the field dependence of F_p should be seen for a microstructure that has large values for both the

COV and the elementary pinning force. For example, this is true for the microstructure Nb-Ti composites. This microstructure has a rather broad distribution in the thickness (t) of the flux-pinning α -Ti precipitates, where $f_p \propto t$,^{17,40} as well as regions in which the precipitates are arranged in clusters.¹⁸ We will explore this further in a moment.

For the entire range of parameters tested, $P(b)$ resembles the function $(1-b)^x$ and $F_p(b)$ the function $b(1-b)^{1+x}$. The value of x is between 0 and 1 for our data. However, closer examination of Fig. 7 reveals that the slope of $P(b)$ does not always vanish as $b \rightarrow 0$ and seems to remain finite as $b \rightarrow 1$. F_p is, then, not simply proportional to $b(1-b)^{1+x}$, and it would be incorrect to infer the field dependence of the pinning mechanism by simply dividing the F_p data by $b(1-b)^x$. Unfortunately, such a procedure is commonly undertaken. For example, the higher-power tail in the field dependence of F_p that is sometimes observed near $b = 1$ can be attributed to variations in B_{c2} or to the saturation of the pinning forces.^{19,41} However the tail may also be due to the presence of a field dependent F_p which is more complicated than a power of $(1-b)$. Additionally, our results suggest that a fit of experimental F_p data over a limited range of b may give a different function than that for $0 \leq b \leq 1$, which would not be the case if F_p were proportional to $b(1-b)^{1+x}$ for all b . An alternative analysis is to note that the $\langle f_p \rangle_{\text{occ}}$ data in Figs. 4 and 5 appear to be the function $(1+x)-b$, which is the Taylor expansion to linear accuracy of $(1-b)^{1+x}$. For example, a much more satisfactory fit of the experimental F_p data in Ref. 42 is obtained with $b(1.5-b)$ than with the scaling function that was reported, $b(1-b)^{1.5}$.

C. An example: The field dependence of F_p for an optimized Nb-Ti composite

In a previous paper,³⁵ we have applied these ideas to the nonscaling of F_p observed in a recent study of a Nb 48 wt. % Ti composite superconductor conducted by Meingast, Lee, and Larbalestier.^{17,18} We wish to undertake a more thorough study here. In the microstructure of that Nb-Ti composite, ribbonlike precipitates of nearly pure titanium are the dominant feature, as seen by transmission electron microscopy. Figure 9 shows an example of the microstructure seen. Here, the precipitates (the lighter phase) have an average thickness of about 2 nm and an average separation of about 10 nm; the composite contains about 18 vol % of precipitate. However, the distribution of precipitate thickness and separation is broad: thin (1–2-nm thick) precipitates appear in clusters that are 20 nm or so in size, within which the precipitate separation is 1–4 nm, while thick (3–6-nm thick) precipitates are separated by 5–20 nm from their nearest neighbors. There are several regions where no precipitate is seen within about a 10 nm radius.

Meingast and Larbalestier presented convincing evidence that the core-pinning (δH_c) mechanism operated for $T/T_c = 0.23$ – 0.95 . They achieved agreement (to within a factor of 2) between the experimental flux-

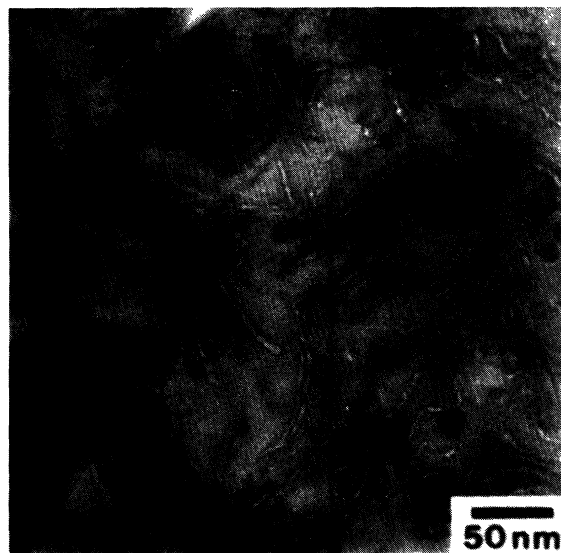


FIG. 9. Transmission electron microscopy micrograph of a Nb 48 wt. % Ti (Nb 64 at. % Ti) composite cross section. The lighter regions are nearly pure titanium precipitates, while the dark gray phase is the superconducting Nb-Ti matrix. The nearly black regions are strongly diffracting Nb-Ti grains. (Photo courtesy of P. Lee).

pinning measurements and their calculations, based on the δH_c mechanism in a slab geometry, at all b for $T/T_c = 0.95$ and for low b at $T/T_c = 0.46$. They were able to obtain the predicted linear dependence on precipitate thickness when $t \lesssim \xi$, as well as the correct temperature scaling exponent, $F_p \propto B_{c2}(T)^{2.0}$. Evidence was also presented to support direct summation, where the agreement between the experiment and the model was good, especially at the high temperature. In the following discussion, we will review their thinking, commenting at times within the framework of our model.

The expected pinning mechanism for the precipitates is the core-pinning mechanism,^{3,6,8,40} f_p being proportional to both t and the relative variation in the critical field ($\delta H_c/H_c$) between the (normal) precipitate and the surrounding (superconducting) matrix. However, since the scaling length for the proximity effect is ξ (about 5.3 nm at 4.2 K for this composite), all the precipitates should be proximity coupled to some degree. The flux pinning is then determined within these coupled, ξ -thick regions, which may not correspond to the boundaries of the precipitates.^{8,40} The magnitude of f_p is determined by the difference between the H_c values of the superconducting matrix, and within the pinning regions. We note that the value of H_c in these coupled regions may be significantly greater than zero. A small enhancement of the pinning occurs because of the proximity effect^{8,40} ($\approx 20\%$, as calculated in the latter reference), which will be ignored.

Assuming that the precipitates are proximity coupled, then the corresponding value of δH_c can be estimated using the average composition within, and next to, the pins. Since titanium is removed from the Nb-Ti matrix during the precipitation process, the matrix phase actually has a composition of about Nb 39 wt. % Ti for 18 vol % of precipitate. This is in contrast to the effective composition

averaged over precipitates and matrix within a radius ξ . At 4.2 K, i.e., $T/T_c \approx 0.46$, this effective composition is Nb 65 wt. % Ti if the average thickness and separation of the precipitates is used. Figure 10(a) shows that the H_c values of the matrix and pinning center are about 1.03 and 0.48 of the value for Nb 48 wt. % Ti, respectively, therefore making $\delta H_c/H_c$ about 0.55.

If we reexamine the microstructure at higher temperature, (e.g., $T/T_c = 0.95$), a rather different picture emerges. This situation is addressed in Fig. 10(b). Since ξ is now about 18 nm, entire clusters of precipitates may become coupled, in addition to the coupling of the isolated precipitates. The clusters are composed of 30–50 % precipitate, giving them average compositions in the range Nb 55–63 wt. % Ti. By comparison, the isolated-precipitate regions would have a composition of about Nb 42–44 wt. % Ti and the precipitate-free matrix regions Nb 39 wt. % Ti. This would lead to two characteristic values of $\delta H_c/H_c$, about 1.5 for the clusters and about 0.2 for the isolated precipitates. The pinning by the precipitate clusters should then dominate because the clusters occur with roughly equal number density as the isolated precipitates.

Since there is a strong δH_c interaction at both temperatures, it is reasonable to expect its characteristic field

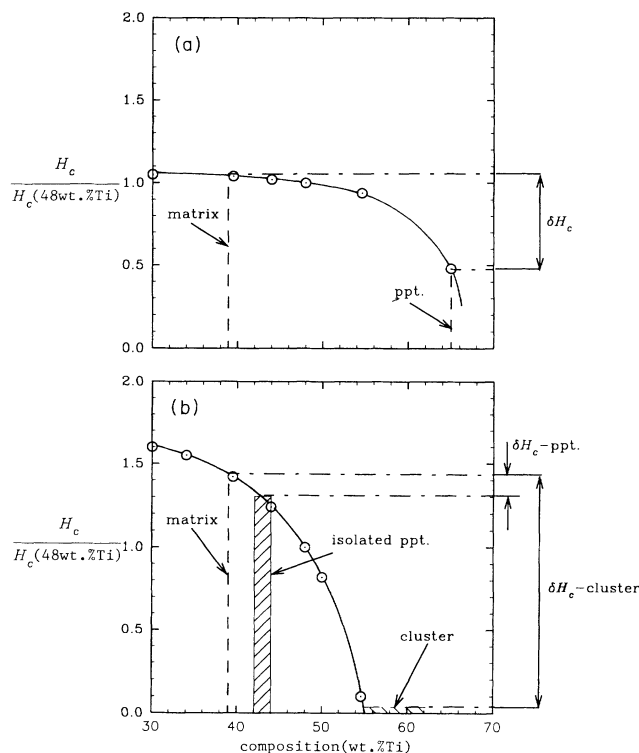


FIG. 10. Normalized (to the value of Nb 48 wt. % Ti) plots of H_c at $T/T_c = 0.46$ (a) and 0.95 (b) as a function of composition. The dashed vertical lines and hatched regions represent the compositions of the matrix and pinning center in each case. The dot-dashed lines represent the corresponding H_c values when the fluxon is within the matrix and when it occupies the pin. The data were taken from Refs. 17, 26, and 27. The abbreviation "ppt." is used for "precipitate."

dependence, $\propto b(1-b)$, to be found in the $F_p(b)$ curves. Unfortunately, this is not the case. Figure 11 shows the data that were actually observed.^{17,27} A shift in the peak of these normalized $F_p(b)$ curves to lower fields is clearly indicated as $T \rightarrow T_c$, starting near the expected value of 0.5 at low temperatures and moving to near 0.3 at $T/T_c = 0.95$.

In terms of our model, the value of f_{p0} appropriate to low temperatures would be about 0.1, since $\delta H_c/H_c \approx 0.55$ and the precipitate thickness is about 0.2ξ . For high temperatures, a value of 2.0 for f_{p0} is reasonable. It is not clear what the COV should be at either temperature; however, it is reasonable to hypothesize that the COV is larger at higher temperatures due to the variation in cluster size and the small contribution of isolated precipitates (Fig. 10). The results of the model prediction are shown in Fig. 12. We have chosen the COV to be 0.1 for low temperatures and 0.5 at $T/T_c = 0.95$. An intermediate curve for $f_{p0} = 0.5$ has been added to estimate the $T/T_c = 0.65$ curve. The agreement between the curves in this figure and those in Fig. 11 is remarkable, especially since the pinning mechanism has not been changed.

In summary, we believe that the preferential pin occupation scheme described here provides a physically reasonable basis for explaining the lack of temperature scaling in the important case of the strongly pinning Nb-Ti system. This system is important because of its practical importance and because extensive microstructural descriptions of the optimized pinning state have been provided. Excellent support for an elementary core pinning interaction came from full-summation calculations, from the temperature scaling exponent, and from the

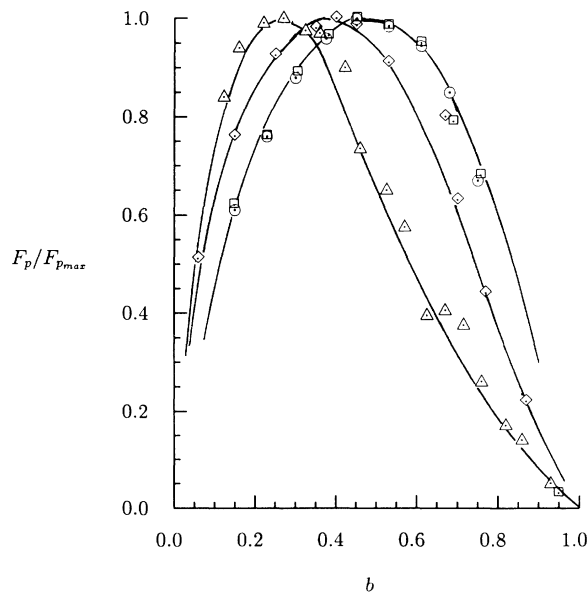


FIG. 11. The reduced F_p data measured for a Nb 48 wt. % Ti composite containing about 18 vol % of precipitate, as a function of b , at $T/T_c = 0.23$ (\odot), 0.46 (\square), 0.65 (\diamond), and 0.95 (\triangle). Note that the \odot and \square curves coincide. The data was taken from Refs. 17 and 27.

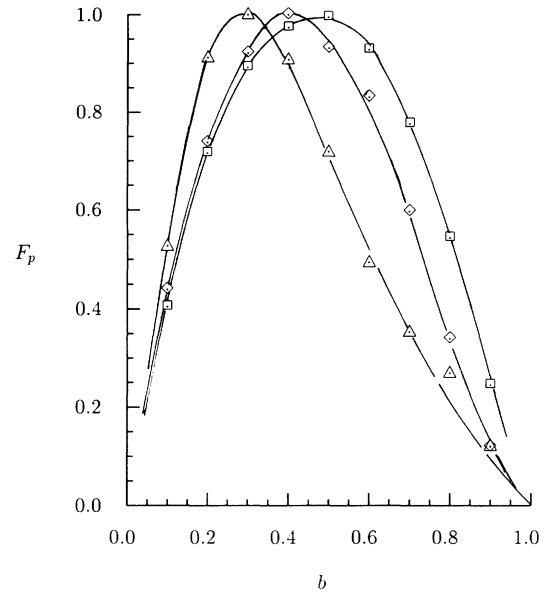


FIG. 12. Reduced F_p curves derived from the $P(b)$ calculations for 20 vol % of pins and the values of f_{p0} and the coefficient of variation equal to 0.1, 0.1 (\square); 0.5, 0.1 (\diamond); and 2.0, 0.5 (\triangle), respectively.

thickness dependence of the elementary pinning interaction. However, all of this has been cast into doubt, because it was precisely in the high-temperature limit, where the core-pinning calculations were most accurate, that the $F_p(b)$ curve deviated most strongly from the expected $b(1-b)$ dependence. This point is fundamental: the easiest of all flux-pinning measurements is that of the $F_p(b)$ curve, and it is entirely understandable that conclusions, albeit wrong ones, will be drawn from the shape of this curve. We have here analyzed these issues for Nb-Ti alloys; it may be that similar effects occur in other superconductor systems.

VI. CONCLUSIONS

We have proposed that statistical variations in the elementary pinning force can lead to filling of the f_p distribution with a preferential hierarchy. This may lead to a difference between the average strength of the occupied pins and the average of the f_p distribution. The difference between these two values vanishes as the field approaches B_{c2} , when the f_p distribution is almost full. Consequently, the average strength of the occupied pins decreases more rapidly with increasing field than would be expected from a calculation based on the operating pinning mechanism. This result is crucial, because the experimentally determined bulk pinning force is proportional to the average strength of the occupied pins. $F_p(b)$ can then appear to be a more strongly field-dependent function than its elementary pinning mechanism would suggest. Our results suggest that the peak of the bulk-pinning-force curve moves to lower field and that its shape has more curvature at high fields. This effect may

lead one to attribute variations in $F_p(b)$ to a change in the pinning mechanism when, in fact, no change has occurred. Finally, we wish to emphasize that our model may hold regardless of the pinning mechanism when the pinning is in the single-fluxon limit, that is, when the pinning interactions are uncorrelated and when their length scale is small enough so as not to compete with the magnetic forces between vortices.

ACKNOWLEDGMENTS

We are deeply appreciative of discussions with Dr. S. Takács during the early stages of this study. We would also like to thank Dr. E. H. Brandt, Dr. P. H. Kes, Dr. A. Gurevich, P. D. Jablonski, and J. L. Vargas for their comments. This work was funded by the U.S. Department of Energy, Division of High Energy Physics.

*Also at Department of Physics.

†Also at Department of Materials Science and Engineering.

¹W. A. Fietz and W. W. Webb, Phys. Rev. **178**, 657 (1969).

²A. M. Campbell and J. E. Evetts, Adv. Phys. **21**, 199 (1972).

³Hans Ullmaier, *Irreversible Properties of Type II Superconductors*, Springer Tracts on Modern Physics, Vol. 76 (Springer-Verlag, Berlin, 1976).

⁴E. J. Kramer, J. Appl. Phys. **44**, 1360 (1973).

⁵D. Dew-Hughes, Philos. Mag. B **30**, 293 (1974).

⁶Teruo Matsushita, Jpn. J. Appl. Phys. **20**, 1153 (1981); **20**, 1955 (1981).

⁷Wilson E. Yetter, Donald A. Thomas, and Edward J. Kramer, Philos. Mag. B **46**, 523 (1982).

⁸T. Matsushita, J. Appl. Phys. **54**, 281 (1983).

⁹D. Dew-Hughes, Philos. Mag. B **55**, 459 (1987).

¹⁰A. M. Campbell, J. Phys. C **4**, 3186 (1971).

¹¹Edward J. Kramer, J. Appl. Phys. **49**, 742 (1978).

¹²Teruo Matsushita, Jpn. J. Appl. Phys. **18**, 1575 (1979).

¹³A. I. Larkin and Yu. N. Ovchinnikov, J. Low Temp. Phys. **34**, 409 (1979).

¹⁴P. H. Kes, D. De Klerk, G. P. Van Der Mey, and J. Bressers, J. Nucl. Mater. **72**, 40 (1978).

¹⁵P. H. Kes and C. C. Tsuei, Phys. Rev. Lett. **47**, 1930 (1981).

¹⁶D. P. Hampshire, A. F. Clark, and H. Jones, J. Appl. Phys. **66**, 3160 (1989).

¹⁷C. Meingast and D. C. Larbalestier, J. Appl. Phys. **66**, 5971 (1989).

¹⁸C. Meingast, P. J. Lee, and D. C. Larbalestier, J. Appl. Phys. **66**, 5962 (1989).

¹⁹T. Matsushita and H. Küpfer, J. Appl. Phys. **63**, 5048 (1988).

²⁰P. H. Kes, Physica C **185-189**, 288 (1991).

²¹J. L. Vargas and D. C. Larbalestier, Appl. Phys. Lett. **60**, 1741

(1992).

²²W. Wordenweber and M. O. Abd-El-Hamed, Supercond. Sci. Technol. **5**(1S), 113 (1992).

²³P. H. Kes and J. Van Den Berg, in *Studies in High-Temperature Superconductors*, edited by A. Narlikar (NOVA Science Publishers, New York, 1990), Vol. 5, p. 83.

²⁴M. Tachiki and S. Takahashi, Solid State Commun. **70**, 291 (1989); Physica C **162-164**, 241 (1989).

²⁵K. E. Gray, R. T. Kampwirth, D. J. Miller, J. M. Murduck, D. Hampshire, R. Herzog, and H. Wever, Physics C **174**, 340 (1991).

²⁶J. C. McKinnell, Ph.D. thesis, University of Wisconsin, 1990.

²⁷C. Meingast, Ph.D. thesis, University of Wisconsin, 1988.

²⁸P. J. Lee and D. C. Larbalestier, J. Mater. Sci. **23**, 3951 (1988).

²⁹P. J. Lee and D. C. Larbalestier, Acta Metall. **35**, 2523 (1987).

³⁰C. W. Hagen and R. Griessen, Phys. Rev. Lett. **62**, 2857 (1989).

³¹R. Griessen, Phys. Rev. Lett. **64**, 1674 (1990).

³²A. Gurevich, Phys. Rev. B **42**, 4857 (1990).

³³S. Martin and A. F. Hebard, Phys. Rev. B **43**, 6253 (1991).

³⁴L. Niel and J. E. Evetts, Europhys. Lett. **15**, 453 (1991).

³⁵L. D. Cooley, G. Stejic, D. C. Larbalestier, and S. Takács, Supercond. Sci. Technol. **5** (1S), 97 (1992).

³⁶E. H. Brandt, Phys. Lett. A **77**, 484 (1980).

³⁷E. H. Brandt, Phys. Rev. B **34**, 6514 (1986).

³⁸E. H. Brandt, Physica C **180**, 426 (1991).

³⁹E. H. Brandt, Int. J. Phys. B **5**, 751 (1991).

⁴⁰G. Stejic, L. D. Cooley, R. Joynt, D. C. Larbalestier, and S. Takács, Supercond. Sci. Tech. **5**(1S), 176 (1992).

⁴¹H. Küpfer and T. Matsushita, J. Appl. Phys. **63**, 5060 (1988).

⁴²L. D. Cooley, P. J. Lee, and D. C. Larbalestier, IEEE Trans. Magn. **27**, 1096 (1991).

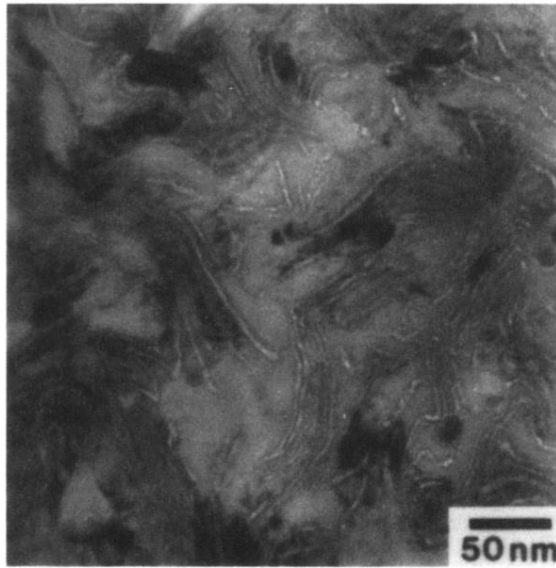


FIG. 9. Transmission electron microscopy micrograph of a Nb 48 wt. % Ti (Nb 64 at. % Ti) composite cross section. The lighter regions are nearly pure titanium precipitates, while the dark gray phase is the superconducting Nb-Ti matrix. The nearly black regions are strongly diffracting Nb-Ti grains. (Photo courtesy of P. Lee).